Hindawi
Advances in Meteorology
Volume 2019, Article ID 8293062, 9 pages
https://doi.org/10.1155/2019/8293062

Research Article

Numerical Simulation of the Effect of Cloud Condensation Nuclei Concentration on the Microphysical Processes in Typhoon Usagi

Xiying Ye,[1,2] **Qimin Cao**,[1] **Baolin Jiang**,[1] **and Wenshi Lin**[1,3]

[1]*School of Atmospheric Sciences, Sun Yat-sen University, Guangzhou 510275, China*
[2]*Guangzhou Meteorological Observatory, Guangzhou, Guangdong 511430, China*
[3]*Guangdong Province Key Laboratory for Climate Change and Natural Disaster Studies, Sun Yat-sen University, Guangzhou 510275, China*

Correspondence should be addressed to Qimin Cao; caoqm@mail2.sysu.edu.cn, Baolin Jiang; jiangblin@mail.sysu.edu.cn, and Wenshi Lin; linwenshi@mail.sysu.edu.cn

Received 3 October 2018; Revised 19 December 2018; Accepted 6 January 2019; Published 12 February 2019

Academic Editor: Ismail Gultepe

The Weather Research and Forecasting model version 3.2.1 with the Lin microphysics scheme was used herein to simulate super typhoon Usagi, which occurred in 2013. To investigate the effect of the concentration of cloud condensation nuclei (CCN) on the development of typhoon Usagi, a control simulation was performed with a CCN concentration of 100 cm^{-3}, together with two sensitivity tests: C10 and C1000, having CCN concentrations of 10 cm^{-3} and 1000 cm^{-3}, respectively. The path, intensity, precipitation, microphysical processes, and the release of latent heat resulting from the typhoon in all three simulations were analyzed to show that an increase in CCN concentration leads to decreases in intensity and precipitation, an increase of the cloudless area in the eye of the typhoon, a more disordered cloud system, and less latent heat released through microphysical processes, especially the automatic conversion of cloud water into rainwater. Overall, an increase in CCN concentration reduces the total latent heat released during the typhoon suggesting that typhoon modification by aerosol injection may be optimized using numerical simulations to ensure the strongest release of latent heat within the typhoon.

1. Introduction

As one of the most important disaster weather phenomena, torrential rain resulting from typhoons has been studied from different perspectives [1–4], but with the consistent goal of understanding the generation mechanisms and development of typhoons, and especially the formation of torrential rain, with the help of numerical simulations. In the 1950s, a numerical procedure for the simulation of the development of tropical cyclones based on a barotropic model was proposed by Kasahara [5, 6]. Next, the development of a typhoon was simulated using a three-level, three-dimensional model, which obtained a spatial structure consistent with observations in [7]. The eye-wall structure of a tropical cyclone was simulated by using a nested mesh model in Kurihara and Bender [8]. Numerical simulation in Lin et al. [9] established the degree to which the vertical vapor flux is affected by terrain and its importance for the prediction of typhoon precipitation. Simulations also identified that evaporation of marine spray caused by the typhoon influences the heat exchange between the typhoon and the sea surface, leading to the convective inhibition of eye-wall motions, and thus a weakening of the typhoon [10]. Mesoscale atmospheric numerical modeling has developed considerably since the 1980s. Beginning around 1997, scientists from several research institutes in the United States jointly developed a new generation of high-resolution mesoscale forecasting models, including the Advanced Research Weather Research and Forecasting (WRF) model [11], which has since been widely used in practical applications.

The impact of cloud condensation nuclei (CCN) on cloud microphysical processes is handled by the cloud microphysics scheme in numerical models. A squall-line process was simulated over Guangdong, China, using the WRF model with three different concentrations of CCN and found that an increase in CCN concentration delays

precipitation, weakens the initial precipitation, and lessens the amount of precipitation for high CCN concentrations [12]. Furthermore, an increase in CCN concentration leads to increases of cloud water and snow and the decrease of sleet [13]. Lin et al. [14] simulated the typhoon Chanchu using the MM5 model to compare the effects of different CCN concentrations; they found that the cloud water growth increases with the concentration of CCN, leading to a positive relationship between the cloud-water mixing ratio and CCN concentration.

Cloud microphysics account for the transformation of hydrometeors, with their overall effect directly impacting the performance of model simulations. Cloud microphysics schemes include, for example, the Lin et al. [15–17], WSM3 [18, 19], WSM6 [20], Ferrier [21], Thompson et al. [22], and Morrison et al. [23] schemes. Niu and Yan [24] simulated a typical precipitation process in the Jianghuai area of China using the WRF model version 2.1.2 and compared the predictions of heavy rainfall based on the Lin, WSM3, WSM6, Ferrier, and Thompson cloud microphysical schemes, with the Lin scheme giving the best performance. Li et al. [25] simulated deep convection over the Tiwi Islands in northern Australia and compared simulations using both Lin and WSM6 schemes, finding a better agreement between simulation results and observations for the Lin scheme. Khin and Min [26] showed that the Lin microphysical scheme produced more heating within the 300–100 hPa layer compared to both Ferrier and WSM6 schemes, producing storms with greater intensity.

Typhoon Usagi is simulated herein with the help of several sensitivity experiments performed using the WRF model version 3.2.1 to explore the effects of CCN concentration on the typhoon track, intensity, and cloud microphysical processes; these aspects are evaluated using the development and movement of the typhoon, as well as the resulting precipitation.

2. Typhoon Development and Simulation Strategy

2.1. Typhoon Development. Super typhoon Usagi was originally formed to the east of the Philippines in the northwestern Pacific Ocean; it continued to build intensity, while slowly moving to the west, after evolving into a tropical storm at 0200 UTC on 17 September 2013. After strengthening to a strong tropical storm at 0800 UTC on 17 September and then a typhoon at 2100 UTC on 17 September, Usagi continued to move westward. On 19 September, typhoon Usagi intensified dramatically, causing the minimum pressure at the typhoon center to decrease from 965 hPa to 950 hPa; thus, it was upgraded to a super typhoon at 1100 UTC. Usagi moved west-northwestward at a maximum wind speed of 60 $m \cdot s^{-1}$, with the minimum pressure reaching 915 hPa near the typhoon center as the typhoon continued to strengthen on 20 September. Passing through the Bashi Channel and entering the northeastern South China Sea, Usagi weakened to a strong typhoon at 2000 UTC on 21 September. On 22 September, typhoon Usagi continued to move west-northwestward and landed at the coastal city of Shanwei in Guangdong Province, at 1900 UTC, with a maximum wind speed of 45 $m \cdot s^{-1}$ and a minimum pressure of 935 hPa. Usagi rapidly weakened on 23 September and gradually dissipated over Guangxi Province. Figure 1(d) presents the 24 h practical accumulated precipitation during the period of strongest precipitation over land. Generally, the distribution of precipitation within Guangdong decreased from east to west, with Shantou City receiving the maximum precipitation of 200 mm.

2.2. Simulation Strategy. The WRF model version 3.2.1 was operated with a Mercator map projection of twin nested grids, with a horizontal grid spacing of 9 km for domain 1 (D01) and 3 km for domain 2 (D02) (Figure 2). The Lin scheme [15] was selected as the cloud microphysics scheme. The rapid radiation transfer model long-wavelength and Goddard short-wavelength radiation parameterizations were used in both domains. The G3 cumulus parameterization was applied in D01, while no cumulus parameterization was applied in D02 because the 3 km grid resolution could not distinguish cumulus processes at the cloud scale. Uncertainty of the cumulus parameterization scheme was much greater than that of the explicit cloud scheme. Typically, the latter scheme describes cloud microphysical processes better and more reasonably represents cloud structure [27]. The 6 h FNL (final) analysis data provided by the National Centers for Environmental Prediction (NCEP)/National Center for Atmospheric Research (NCAR) with 1° horizontal resolution were used as the initial field of the model. The modeling period in the D01 domain amounted to 84 h from 1200 UTC on 19 September 2013 to 0000 UTC on 23 September 2013. The modeling period in the D02 domain amounted to 60 h from 1200 UTC on 20 September 2013 to 0000 UTC on 23 September 2013. The integral time steps of domains D01 and D02 were 30 s and 10 s, respectively.

In the Lin scheme, the cloud droplet number concentration (N_c), which represents the CCN concentration, was set to 100 cm^{-3} in the control test (CTL) but varied in the sensitivity tests (C10, C1000) to reflect clean-air and heavy air pollution scenarios, with all other parameters held constant.

3. Results

3.1. The Effect of Cloud Condensation Nuclei Concentration. Figure 3 compares the simulated paths of all three experiments with the actual path of the typhoon. While the simulated landfall sites in the three experiments deviate from the observed landfall site, the simulated paths are largely consistent, with each other and with the observed path. Figure 4 compares the simulated sea-level pressure in all three experiments with pressures observed. Initially, the simulated intensity was weaker than that observed. Consequently, simulations gave a reduced typhoon speed compared to that observed. The comparison of the three simulations indicates that the lowest sea-level pressure increases with increasing CCN concentration, with the lowest sea-level pressure simulated in C1000 being consistently higher (by 2 hPa) than that in C10, as well as in the C100 case. Therefore, the typhoon intensity in the simulations decreased with increasing CCN concentration.

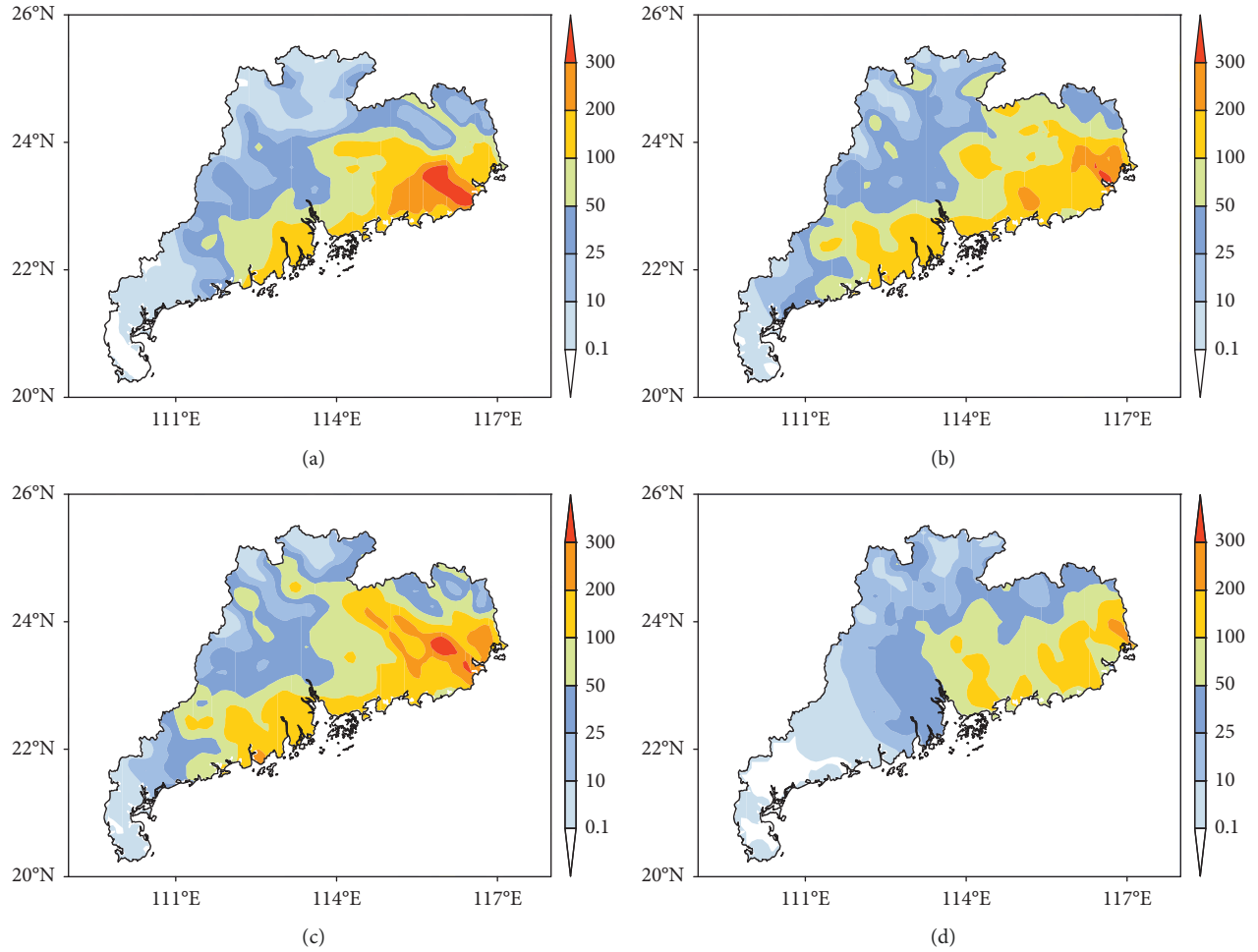

Figure 1: Comparison of 24 h accumulated precipitation in C10 (a), C1000 (b), and C100 (c) runs with observations (d) at 0000 UTC on 23 September.

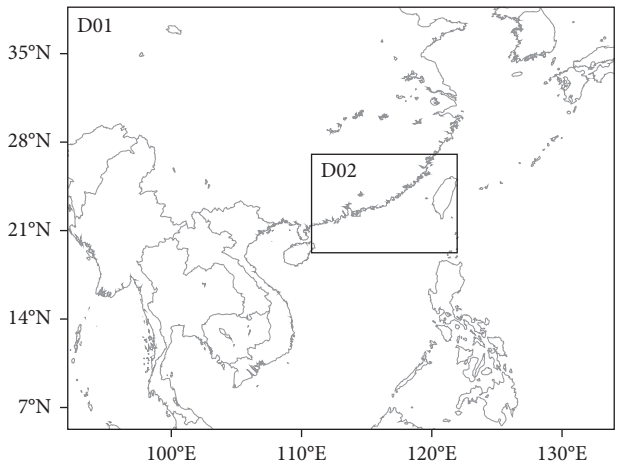

Figure 2: Position of the nested domain D02 within domain D01 in the Weather Research and Forecasting model version 3.2.1 simulations.

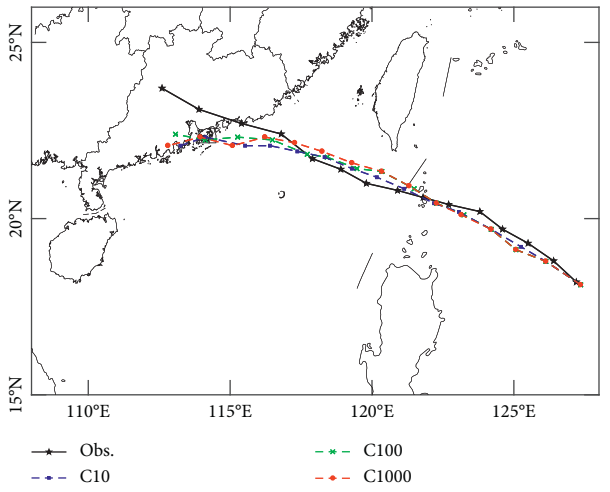

Figure 3: Comparison of the simulated typhoon paths with observations (black) for the C10 (blue), C100 (green), and C1000 (red).

3.2. The Effect of Cloud Condensation Nuclei Concentration on the Usagi Precipitation Simulation. Figure 1 compares the 24 h accumulated precipitation on land in the CTL experiment with that observed; it shows that the amount of precipitation reached a maximum in the CTL experiment of over 300 mm, which is larger than that observed. In terms

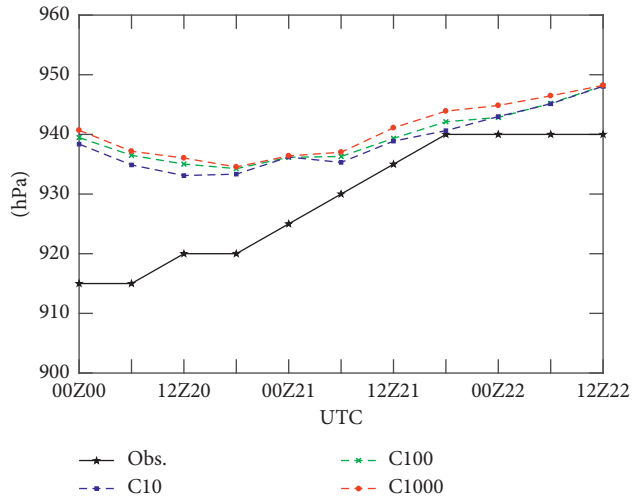

FIGURE 4: Comparison of simulated minimum sea-level pressures with observations for the C10, C100, and C1000 runs.

of the spatial distribution of precipitation, the area of torrential rain (24 h accumulated precipitation of more than 100 mm) in the CTL simulation contradicts the observations to the west of the Pearl River Delta region (resulting from the deviation of the typhoon path) but is consistent with observations to the east of the Pearl River Delta region. In addition, the heavy rain (24 h accumulated precipitation less than 50 mm) area in the CTL results approximates observations in North Guangdong, but with lower precipitation levels in North and West Guangdong. Contrasting this with the sensitivity tests, in the case of C10, large values of precipitation of more than 300 mm are centered to the west of Shantou City (116.2°E, 23.2°N), but with a reduced area in the CTL experiment; this disappears in the results for C1000. Moreover, the region of approximately 200–300 mm precipitation is significantly reduced in C1000. Therefore, the precipitation decreased with increasing CCN concentration.

3.3. The Effect of Cloud Condensation Nuclei Concentration on Radar Reflectivity and the Distribution of Cloud-Top Temperature. Figure 5 compares the simulated radar maximum reflectivity with that observed at 0000 UTC on 22 September. While much larger eye-wall regions are evident in all three experiments compared with that observed, the strong radar reflectivity observed in the northern part of the typhoon close to land was captured correctly. The typhoon eye area increased with increasing CCN concentration, according to the three experiments, with C10 producing a larger area of radar reflectivity (>50 dBZ) compared with the CTL and C1000 runs.

Figure 6 shows the distribution of cloud-top temperature in all three experiments at 0000 UTC on 22 September. Clearly, the cloud-top temperature was highest in C1000, followed by the CTL and C10 runs, indicating a decrease of the cloud-top height within the typhoon with increasing CCN concentration. The cloud cover in C10 is more evenly distributed in contrast to the fragmented clouds in the eye-wall region in the CTL run and the disconnected regions of large-scale cloud cover in C1000. Because the magnitude of the CCN concentration affects the distribution of cloud cover, this indicates the importance of CCN to the development of typhoon intensity and precipitation.

3.4. The Effect of Cloud Condensation Nuclei Concentration on the Conversion of Cloud Microphysical Parameters. By concentrating on domain D02 (3 km resolution) and periods when the typhoon was still located offshore (from 1700 UTC to 2200 UTC on 21 September) as well as when the typhoon made landfall (from 1500 UTC to 2000 UTC on 22 September), the effect of CCN concentration on typhoon development was analyzed in detail by considering the vertical integral of a particular conversion parameter [28],

$$[P_x] = \sum_{i,j,k} p_x(i,j,k) \times \rho(i,j,k) \times \Delta z(k), \quad (1)$$

where $[P_x]$ is the vertical integral of the microphysical process X, ρ is the density of air (kg·m^{-3}), Δz is the distance between the adjacent layers in the vertical direction, and p_x is the hourly microphysical conversion on each grid (kg·kg^{-1}·h^{-1}).

Table 1 shows results of the vertical integration using equation (1) of the microphysical conversions in domain D02 for all three experiments in both periods. The cloud microphysical conversions within the period when the typhoon made landfall are smaller than those within the period when the typhoon was offshore, which indicates that the typhoon weakened. This is probably related to the increased friction of the underlying surface, as the typhoon passed through the Bashi Channel. The microphysical processes correspondingly slowed, along with the weakening of the typhoon. Most cloud microphysical conversions decreased with increasing CCN concentration, except for the CEVP process (the conversion of cloud water to vapor related to evaporation). In this case, cloud water decreased, which is conducive to reducing precipitation.

The automatic conversion of cloud water to rain in the Lin scheme [15] is calculated by

$$P_{\mathrm{RAUT}} = \rho (l_{\mathrm{CW}} - l_{\mathrm{W0}})^2 \left[1.2 \times 10^{-4} + \left\{ \frac{1.569 \times 10^{-12} N_1}{D_0 (l_{\mathrm{CW}} - l_{\mathrm{W0}})} \right\} \right]^{-1}, \quad (2)$$

where N_1 and l_{CW} represent the number concentration of cloud droplets and the cloud-water mixing ratio, respectively; l_{W0} (2×10^{-3} g·g^{-1} in the model) represents the automatic conversion threshold; and D_0 (a constant in the model) represents the dispersion of the cloud droplet distribution. In reducing the microphysical conversion rate, RAUT (the process whereby cloud water automatically converts to rain) is weakened significantly. In the first period, for example, RAUT decreases significantly from 1.47 mm·h^{-1} to 0.01 mm·h^{-1} with increasing CCN concentration. Equation (2) shows that the increase in CCN concentration (through the increase in N_1) inhibits RAUT, leading to the weakening of cloud microphysical processes relevant to rain. From the microphysical perspective, the

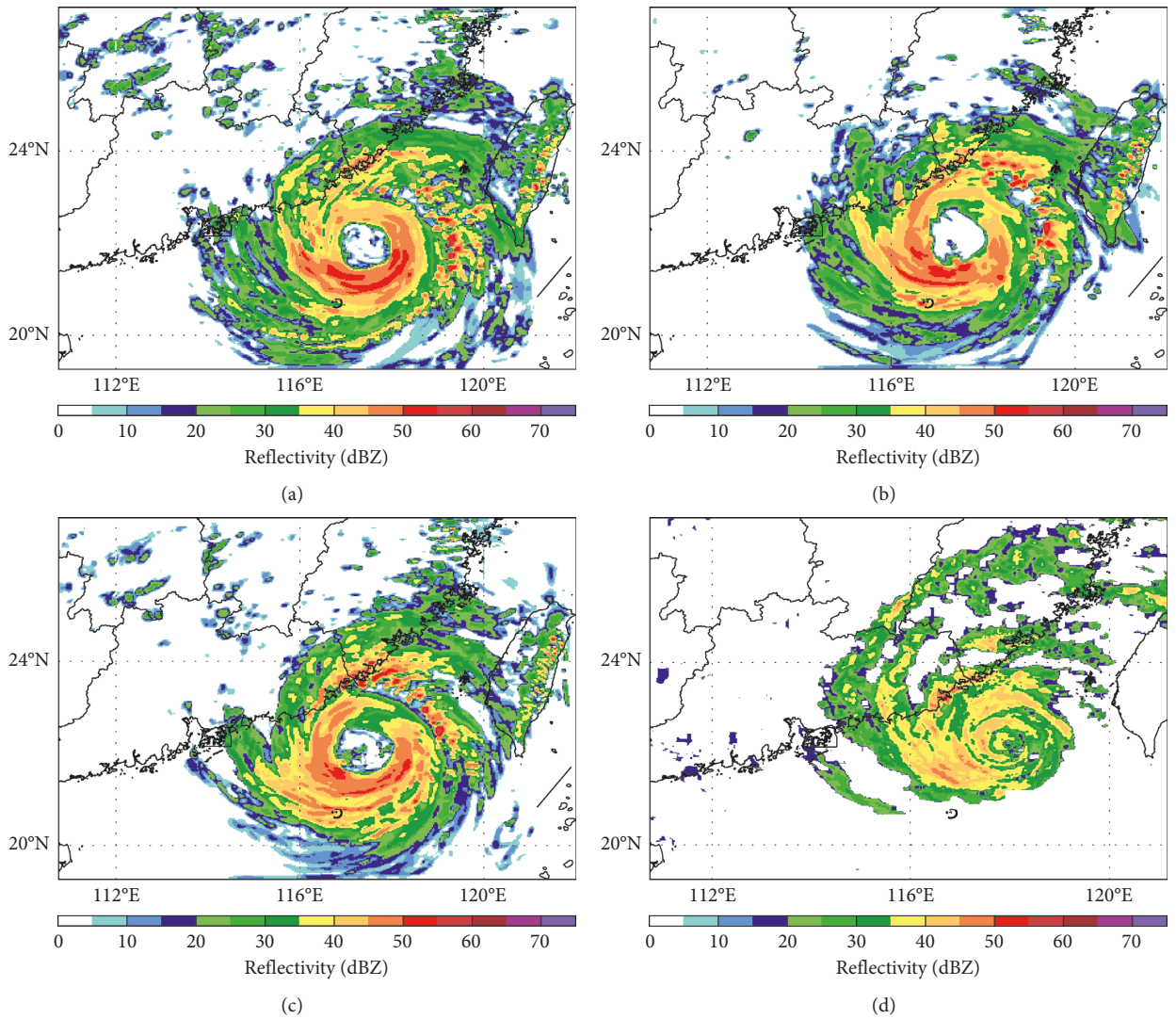

Figure 5: Comparison of radar maximum reflectivity in C10 (a), C1000 (b), and C100 (c) runs with observation (d) at 0000 UTC on 22 September. The radar observation is sourced from the China Weather News.

increasing CCN concentration results in enhanced competition between CCN for the limited water vapor, leading to a decrease in the cloud droplet size. As a result, the probability that cloud droplets automatically convert to larger rain droplets decreases, which is the core process, when considering the physics of the influence of CCN concentration on precipitation.

3.5. The Effect of Cloud Condensation Nuclei Concentration on the Release of Latent Heat during Usagi. The release of latent heat by various microphysical processes is an important aspect in the development of typhoons. Of the 33 cloud microphysical processes in the Lin scheme, 19 are able to produce latent heat through phase transitions resulting from condensation (Q_{con}), evaporation (Q_{evp}), freezing (Q_{frz}), melting (Q_{mlt}), deposition (Q_{dep}), and sublimation (Q_{sub}); these may be calculated at each integral step in the model to obtain the total heat released over a certain period (Q_{total}) using

$$
\begin{aligned}
Q_{con} &= \frac{L_v \times P_{cond}}{C_{pm}},\\
Q_{evp} &= \frac{L_v \times vP_{cevp} + P_{revp} + P_{gmltevp} + P_{smltevp}}{C_{pm}},\\
Q_{frz} &= \frac{L_f \times rP_{ihom} + P_{iacr} + P_{gacr} + P_{sacr}}{C_{pm}},\\
Q_{mlt} &= \frac{L_f \times lP_{smlt} + P_{imlt} + P_{gmlt}}{C_{pm}},\\
Q_{dep} &= \frac{L_s \times eP_{idep} + P_{sdep} + P_{gdep} + P_{idw}}{C_{pm}},\\
Q_{sub} &= \frac{L_s \times uP_{gsub} + P_{ssub} + P_{isub}}{C_{pm}},\\
Q_{total} &= Q_{con} + Q_{evp} + Q_{frz} + Q_{mlt} + Q_{dep} + Q_{sub},
\end{aligned}
\tag{3}
$$

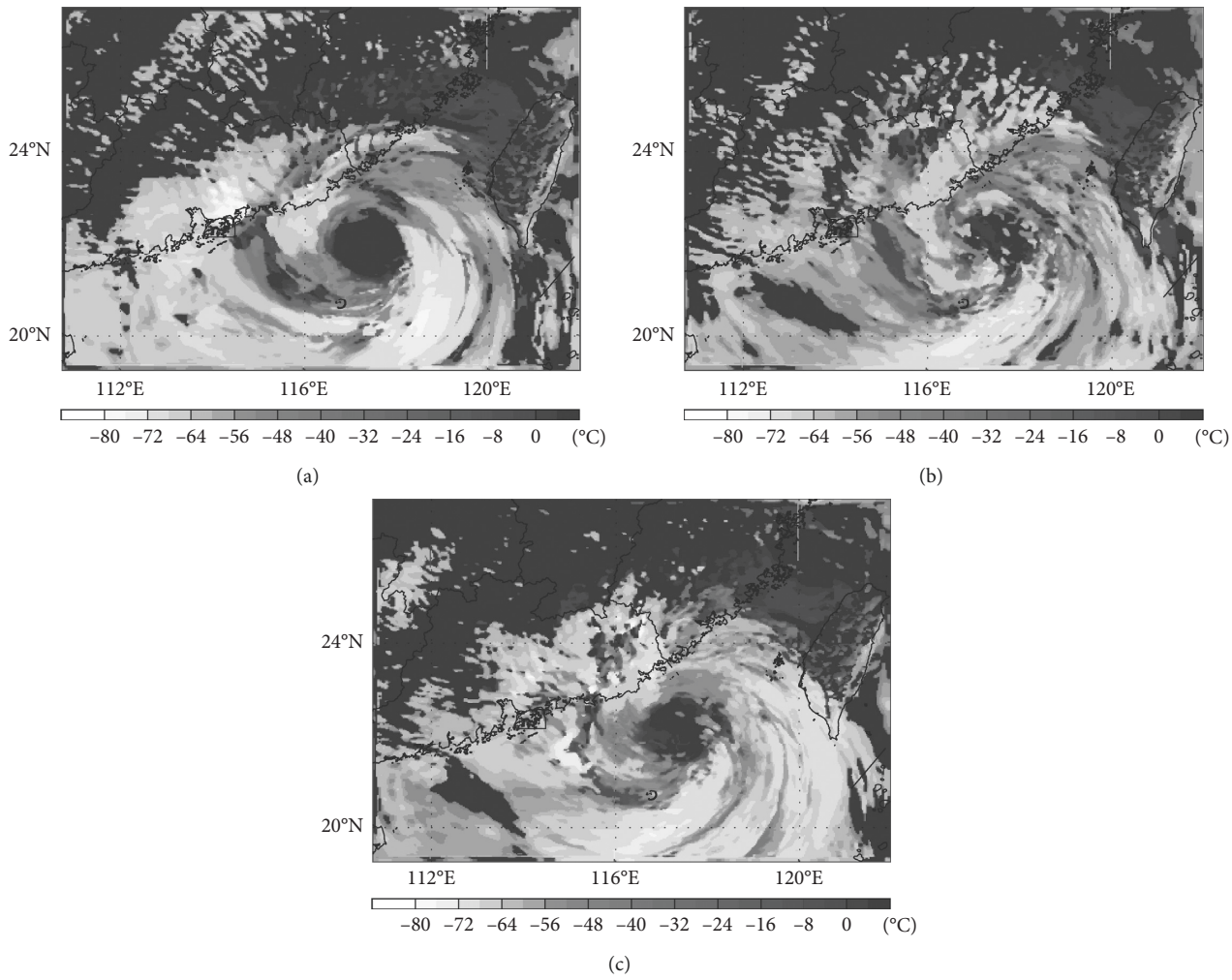

Figure 6: Comparison of the distribution of cloud-top temperature in C10 (a), C1000 (b), and C100 (c) runs at 0000 UTC on 22 September.

where P_X (kg·kg^{-1}·s^{-1}) is the transition rate of a cloud microphysical process; L_v, L_f, and L_s (J·kg^{-1}) are the latent heats of condensation, freezing, and deposition per unit mass, respectively; and C_{pm} (J·kg^{-1}·K^{-1}) is the specific heat of moist air at constant pressure.

The regional time-averaged vertical profile of total latent heat produced from 1200 UTC to 1800 UTC on 22 September in domain D02 (114°E–116°E, 20.5°N–22.5°N) is presented in Figure 7. This illustrates the consistent trend of two peaks, one of which is located at the height of 2 km, and the other between 5 km and 6 km, on the total latent heating rate in all three experiments. Typically, the latent heating rate decreased rapidly at 2–4 km and increased above 4 km. Further analysis of the latent heat contributions (diagram not shown) indicates that the first peak depends mainly on the degree of latent heat from condensation, while the second peak depends mainly on the degree of latent heat from condensation, freezing, and melting. Comparing the three experiments, only the second peak of C10 is larger than the first one. In addition, the total latent heating rate corresponding to the two peaks in C10 is obviously larger than that in the CTL test, which is slightly larger than that in C1000. Hence, an increase of CCN is beneficial to the suppression of the release of latent heat in a typhoon.

The addition of aerosols into the peripheral spiral rain bands of the typhoon is the common mode of typhoon intensity modification, where many CCN reduce the rate of cloud droplets converting into raindrops, which then rise to the height of freezing, creating more supercooled water droplets. The process by which supercooled water droplets convert to ice produces latent heat, triggering convection and enhancing the vertical motion within the spiral cloud belt on the typhoon's periphery. This motion is beneficial to the development of convective clouds and the reduction of the convergence of warm air and heat at the typhoon center. This process increases the radius of the typhoon eye and decreases the maximum wind speed to conserve momentum, resulting in a weakened typhoon [29]. Therefore, typhoon modification by aerosol injection may be optimized using numerical simulations to ensure the strongest release of latent heat within typhoons.

4. Conclusions

The Weather Research and Forecasting model version 3.2.1 with a single nested domain was used in this study to simulate super typhoon Usagi, with a focus on the Lin

Table 1: The effects of C10, C1000, and CTL runs on different microphysical conversions ($mm \cdot h^{-1}$).

Microphysical conversions	The meanings of the microphysical conversions	1700–2100 UTC on 21 September			1500–2000 UTC on 22 September			Trends
		C10	CTL	C1000	C10	CTL	C1000	
GACR	Graupel absorbs rain	22.14	20.53	17.77	8.26	8.03	6.99	↓
COND	Water vapor condenses into cloud water	12.44	12.47	12.00	8.16	8.73	8.22	—
RACW	Rainwater absorbs cloud water	6.08	6.90	6.85	3.67	4.30	4.06	—
GMLT	Graupel melts into rain	5.17	4.96	4.58	2.82	2.96	2.72	—
GACW	Graupel absorbs cloud water	2.72	2.77	2.66	1.38	1.53	1.39	—
GACS	Graupel absorbs snow	1.79	1.73	1.74	1.20	1.18	1.10	↓
IDEP	Cloud ice deposition	1.70	1.68	1.57	1.19	1.15	1.05	↓
REVP	Rainwater evaporates	1.62	1.46	1.38	0.94	0.86	0.76	↓
RAUT	Cloud water automatically converts to rain	1.47	0.30	0.01	0.95	0.22	0.01	↓
SACR	Snow absorbs rain	1.44	1.35	1.26	0.92	1.00	0.96	—
SFI	Snow freezes cloud ice	1.43	1.40	1.30	0.94	0.93	0.86	↓
CEVP	Cloud water evaporates into vapor	1.26	1.43	1.44	1.21	1.53	1.60	↑
GDEP	Graupel deposition	0.61	0.59	0.54	0.31	0.31	0.28	↓
ISUB	Cloud ice sublimation	0.36	0.34	0.32	0.26	0.25	0.23	↓
GSUB	Graupel sublimation	0.17	0.15	0.14	0.08	0.06	0.05	↓
SDEP	Snow deposition	0.16	0.16	0.15	0.12	0.12	0.11	↓
IACR	Cloud ice absorbs rain	0.16	0.09	0.08	0.07	0.05	0.04	↓
RACS	Rain absorbs snow	0.09	0.04	0.02	0.06	0.03	0.02	↓
SACW	Snow absorbs cloud water	0.10	0.10	0.11	0.07	0.07	0.07	—
SACI	Snow absorbs cloud ice	0.07	0.08	0.07	0.05	0.05	0.04	—
SAUT	Cloud ice automatically converts to snow	0.06	0.06	0.05	0.04	0.04	0.03	—
SSUB	Snow sublimation	0.06	0.07	0.06	0.05	0.04	0.03	—
GMLTEVP	Evaporation of melted graupel	0.05	0.03	0.03	0.01	0.01	0.01	—
SFW	Cloud water converts to snow	0.01	0.01	0.01	0.01	0.01	0.01	—
SMLT	Snow melts into rain	0.01	0.01	0.01	0.01	0.01	0.01	—
IHOM	Cloud water homogeneously freezes into cloud ice	0.01	0.01	0.01	0.00	0.00	0.00	—
GACI	Graupel absorbs ice	0.01	0.01	0.01	0.01	0.01	0.01	—
GAUT	Snow automatically converts to graupel	0.00	0.00	0.00	0.00	0.00	0.00	—
GFR	Rain freezes into graupel	0.00	0.00	0.00	0.00	0.00	0.00	—
RACI	Rain absorbs cloud ice	0.00	0.00	0.00	0.00	0.00	0.00	—
IMLT	Cloud ice melts into cloud water	0.00	0.00	0.00	0.00	0.00	0.00	—
IDW	Cloud water sublimates into cloud ice	0.00	0.00	0.00	0.00	0.00	0.00	—
SMLTEVP	Evaporation of melting snow	0.00	0.00	0.00	0.00	0.00	0.00	—

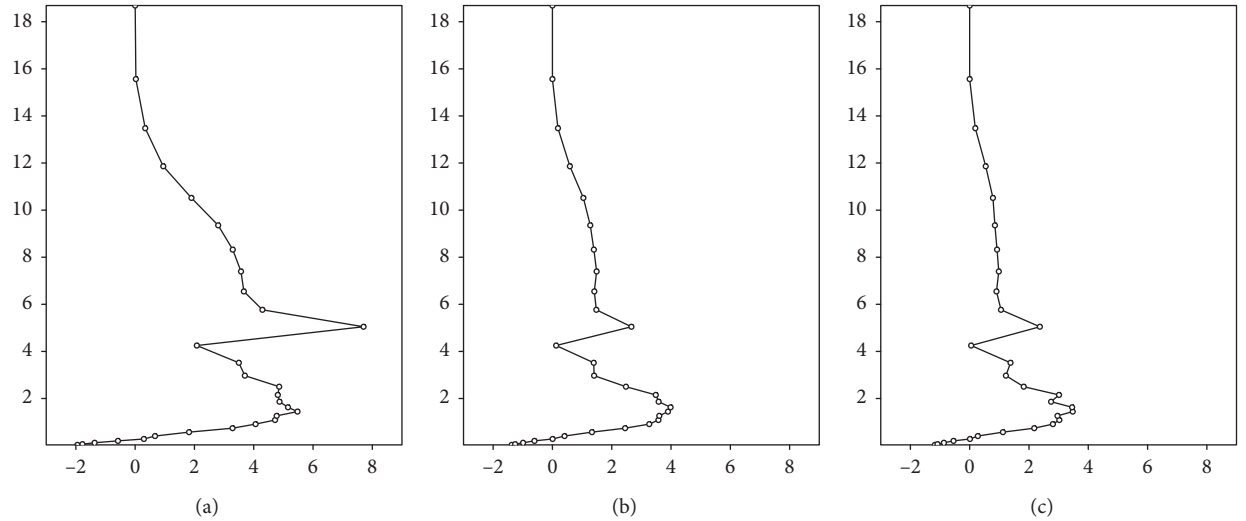

Figure 7: The regional time-averaged vertical profiles of total latent heating rate ($K \cdot h^{-1}$) in C10 (a), C100 (b), and C1000 (c) runs from 1200 UTC to 1800 UTC on 22 September.

scheme as the cloud microphysical scheme for three different CCN concentrations. These simulations showed the following:

(1) The typhoon intensity, precipitation, and cloud-top height decreased with increasing CCN concentration. The distribution of the cloud system also decreased and became more irregular with increasing CCN concentration.

(2) An increasing CCN concentration corresponded to a reduced release of latent heat in most cloud microphysical processes as a result of competition between CCN for the limited water vapor, leading to a decrease in cloud droplet size. Because the probability that cloud droplets are automatically converted to larger-sized rain droplets correspondingly decreases, increasing CCN concentration affects RAUT efficiency (automatic cloud water conversion to rainwater), leading to weakening of the cloud microphysical processes related to precipitation.

(3) The increasing number of CCN suppressed the release of latent heat within the typhoon. Typically, two peaks occurred on the total latent heating curve, with one peak located just below 2 km, dependent on the degree of latent heat from condensation, and the other located at a height of 5-6 km, dependent on the degree of condensation, freezing, and melting. The existence of latent heat peaks may facilitate a new way of parameterizing and analyzing the extent to which latent heat release modifies the strength of typhoons.

As only numerical simulations of a single typhoon have been carried out here, these simulations do not necessarily represent all circumstances. Clearly, further simulations are necessary to broaden our understanding of typhoon dynamics.

Data Availability

The National Center for Atmospheric Research's Mesoscale and Microscale Meteorology Division provided the WRF-Chem model available at http://www.mmm.ucar.edu/wrf/users. The National Centers for Environmental Prediction Final Global Tropospheric Analysis (NCEP-FNL) data were downloaded from https://rda.ucar.edu/datasets/ds083.2. All data used to support the findings of this study are available from the corresponding author upon request.

Conflicts of Interest

The authors declare that they have no conflicts of interest.

Acknowledgments

The authors were supported by the National Key R&D Program of China (2018YFC1507402), National Natural Science Foundation of China (41875168 and 41705117), Natural Science Foundation of Guangdong Province (2015A030311026), and Guangzhou Science and Technology Plan (201707010088).

References

[1] Y. Zhang, W. Meng, G. Dai et al., "The evolution and formation mechanism of rainstorms MCSs during typhoon Fnanpi landing," *Journal of Tropical Meteorology*, vol. 31, no. 4, pp. 433–443, 2015, in Chinese.

[2] D. Han, W. Yan, and J. Ye, "Analyzing cloud, precipitation, and thermal structure characteristics of typhoons in eastern Pacific based on CloudSat satellite data," *Chinese Journal of Atmospheric Sciences*, vol. 37, no. 3, pp. 691–704, 2013, in Chinese.

[3] H. Xu and B. Hu, "The impact of Typhoon Danas (2013) on the torrential rainfall associated with Typhoon Fitow (2013) in east China," *Advances in Meteorology*, vol. 2015, Article ID 383712, 11 pages, 2015.

[4] J. C. H. Fung and G. Gao, "Evaluations on profiles of the eddy diffusion coefficients through simulations of super typhoons in the northwestern pacific," *Advances of Meteorology*, vol. 2016, Article ID 2397873, 14 pages, 2016.

[5] A. Kasahara, "A comparison between geostrophic and non-geostrophic numerical forecasts of hurricane movement with the barotropic steering model," *Journal of Meteorology*, vol. 16, pp. 371–384, 1959.

[6] A. Kasahara, "The numerical prediction of hurricane movement with the barotropic model," *Journal of Meteorology*, vol. 14, no. 5, pp. 386–402, 1957.

[7] R. W. Jones, "A nested grid for a three-dimensional model of a tropical cyclone," *Journal of the Atmospheric Sciences*, vol. 34, no. 10, pp. 1528–1553, 1977.

[8] Y. Kurihara and M. A. Bender, "Structure and analysis of the eye of a numerically simulated tropical cyclone," *Journal of the Meteorological Society of Japan. Ser. II*, vol. 60, no. 1, pp. 381–395, 1982.

[9] Y.-L. Lin, S. Chiao, T.-A. Wang, M. L. Kaplan, and R. P. Weglarz, "Some common ingredients for heavy orographic rainfall," *Weather and Forecasting*, vol. 16, no. 6, pp. 633–660, 2001.

[10] Y. Wang, J. D. Kepert, and G. J. Holland, "The effect of sea spray evaporation on tropical cyclone boundary layer structure and intensity∗," *Monthly Weather Review*, vol. 129, no. 10, pp. 2481–2500, 2001.

[11] X. Wang and H. Ma, "Progress of application of the weather research and forecast (WRF) model in China," *Advances in Earth Science*, vol. 26, no. 11, pp. 1191–1199, 2011, in Chinese.

[12] H. Dong, H. Xu, and Y. Luo, "Effects of cloud condensation nuclei concentration on precipitation in convection permitting simulations of a squall line using WRF model: sensitivity to cloud microphysical schemes," *Chinese Journal of Atmospheric Science*, vol. 36, no. 1, pp. 145–169, 2012, in Chinese.

[13] B. A. Colle and Y. Zeng, "Bulk microphysical sensitivities within the MM5 for orographic precipitation. Part I: the Sierra 1986 event," *Monthly Weather Review*, vol. 132, no. 12, pp. 2780–2801, 2004.

[14] W. Lin, S. Xu, and C.-H. Sui, "A numerical simulation of the effect of the number concentration of cloud droplets on Typhoon Chanchu," *Meteorology and Atmospheric Physics*, vol. 113, no. 3-4, pp. 99–108, 2011.

[15] Y.-L. Lin, R. D. Farley, and H. D. Orville, "Bulk parameterization of the snow field in a cloud model," *Journal of Climate and Applied Meteorology*, vol. 22, no. 6, pp. 1065–1092, 1983.

[16] S. A. Rutledge and P. V. Hobbs, "The mesoscale and microscale structure and organization of clouds and precipitation in midlatitude cyclones. XII: a diagnostic modeling study of precipitation development in narrow cold-frontal

rainbands," *Journal of the Atmospheric Sciences*, vol. 41, no. 20, pp. 2949–2972, 1984.

[17] W.-K. Tao, J. Simpson, and M. McCumber, "An ice-water saturation adjustment," *Monthly Weather Review*, vol. 117, no. 1, pp. 231–235, 1989.

[18] S.-Y. Hong, J. Dudhia, and S.-H. Chen, "A revised approach to ice microphysical processes for the bulk parameterization of clouds and precipitation," *Monthly Weather Review*, vol. 132, no. 1, pp. 103–120, 2004.

[19] J. Dudhia, "Numerical study of convection observed during the winter monsoon experiment using a mesoscale two-dimensional Model," *Journal of the Atmospheric Sciences*, vol. 46, no. 20, pp. 3077–3107, 1989.

[20] S.-Y. Hong, H.-M. H. Juang, and Q. Zhao, "Implementation of prognostic cloud scheme for a regional spectral model," *Monthly Weather Review*, vol. 126, no. 10, pp. 2621–2639, 1998.

[21] Q. Zhao and F. H. Carr, "A prognostic cloud scheme for operational NWP models," *Monthly Weather Review*, vol. 125, no. 8, pp. 1931–1953, 1997.

[22] G. Thompson, R. M. Rasmussen, and K. Manning, "Explicit forecasts of winter precipitation using an improved bulk microphysics scheme. Part I: description and sensitivity analysis," *Monthly Weather Review*, vol. 136, no. 2, pp. 519–542, 2004.

[23] H. Morrison, G. Thompson, and V. Tatarskii, "Impact of cloud microphysics on the development of trailing stratiform precipitation in a simulated squall line: comparison of one- and two-moment schemes," *Monthly Weather Review*, vol. 137, no. 3, pp. 991–1007, 2009.

[24] J. Niu and Z. Yan, "The effect of microphysical schemes of WRF model on heavy precipitation forecast," *Science and Technology Information*, vol. 23, pp. 17–20, 2007, in Chinese.

[25] J. Li, Y. Yin, and L. Jin, "A numerical study on deep tropical convection using WRF model," *Journal of Tropical Meteorology*, vol. 25, no. 3, pp. 287–294, 2009, in Chinese.

[26] W. M. Khin and J. Min, "Impacts of microphysical schemes and topography on the prediction of the heavy rainfall in western Myanmar associated with tropical cyclone ROANU (2016)," *Advances of Meteorology*, vol. 2017, Article ID 3252503, 22 pages, 2017.

[27] Y. Wang, K.-H. Lee, Y. Lin, M. Levy, and R. Zhang, "Distinct effects of anthropogenic aerosols on tropical cyclones," *Nature Climate Change*, vol. 4, no. 5, pp. 368–373, 2014.

[28] I. Gultepe, A. J. Heymsfield, P. R. Field, and D. Axisa, "Ice-phase precipitation," *Meteorological Monographs*, vol. 58, pp. 6.1–6.36, 2017.

[29] D. Rosenfeld and W. L. Woodley, "Deep convective clouds with sustained supercooled liquid water down to −37.5°C," *Nature*, vol. 405, no. 6785, pp. 440–442, 2000.